

# Unified Representation for Machine Learning of Molecules and Crystals

Haoyan Huo

*School of Physics, Peking University, Beijing, China*

Matthias Rupp

*Fritz Haber Institute of the Max Planck Society, Faradayweg 4–6, 14195 Berlin, Germany\**

(Dated: November 10, 2021)

Accurate simulations of atomistic systems from first principles are limited by computational cost. In high-throughput settings, machine learning can potentially reduce these costs significantly by accurately interpolating between reference calculations. For this, kernel learning approaches crucially require a single Hilbert space accommodating any atomistic system. We introduce a many-body tensor representation that has proper mathematical structure, satisfies theoretical requirements, and can represent both molecules and crystals. Empirical evidence is presented for energy prediction errors below 1 kcal/mol for 7 k organic molecules and 3 meV/atom for 11 k elpasolite crystals. Applicability is demonstrated for phase diagrams of Pt-group/transition-metal binary systems.

*Introduction.* Computational study of atomistic systems, including molecules and crystals, requires accurate treatment of interactions at the atomic and electronic scales. Existing first-principles methods, however, are limited by their prohibitive computational cost. In high-throughput settings, machine learning (ML) [1] might significantly reduce overall costs by accurately interpolating between reference calculations. [2, 3] For this, the problem of repeatedly solving a complex equation like Schrödinger’s equation *for many related inputs* is mapped onto a non-linear regression problem: Instead of numerically solving new systems, they are statistically estimated based on a reference set of known solutions. [4, 5] This ansatz potentially enables screening larger databases of molecules and materials [2, 6], running longer dynamics simulations [3], investigating larger systems [7], and even increasing the accuracy of calculations [2, 8].

Kernel-based ML models [9] for accurate prediction of ab initio properties require a single Hilbert space of atomistic systems in which regression is carried out. Representations, that is functions mapping atomistic systems to Hilbert space elements via a kernel [10], should be [5, 11, 12] (i) *invariant* against transformations preserving the predicted property, in particular translation, rotation, and nuclear permutation of same elements, as learning these invariances from data would require many reference calculations; (ii) *unique*, that is variant against transformations changing the property, as systems with identical representation but differing in property would introduce errors [13]; (iii) *continuous*, and ideally differentiable, as discontinuities work against smoothness assumptions of the ML model; (iv) *general* in the sense of being able to encode any atomistic system accepted by the reference method, ideally including finite and periodic systems; (v) *fast to compute*, as the goal is to reduce computational cost; (vi) *efficient* in the sense of requiring few reference calculations to reach a given target error. Constant-size vector representations can be advantageous [14], for example for vector-based kernels.

Current representations such as Coulomb matrix (CM) [4], bag of bonds (BoB) [15], bispectrum [3], smooth overlap of atomic positions (SOAP) [11], symmetry functions [16], bonding angular machine learning [17], and others [12, 18, 19] fulfill these requirements partially. More *ad-hoc* representations, such as many of the descriptors in cheminformatics [20], usually violate (ii) and (iii), in particular if they do not include atomic coordinate information and rely on cut-off-based definitions of chemical bonds. Such descriptors serve the different purpose of interpolating between experimental outcomes, which have strong measurement noise and are not functions of a single conformation. Representations can encode both atoms in their chemical environment (SOAP, symmetry functions) or systems as a whole (CM, BoB). The former are more suitable for predicting local properties like forces and chemical shifts, but require partitioning schemes for global properties such as energy. The latter are suited for global properties, but require modifications to represent local environments.

Here, we introduce a many-body tensor representation (MBTR) derived from the CM/BoB family and concepts from many-body expansions that fulfills the above requirements, has proper mathematical structure (Eq. 3), is interpretable, allows visualization (Fig. 1), and can describe finite and periodic systems. We demonstrate state-of-the-art empirical performance for organic molecules and inorganic crystals, as well as applicability for phase diagrams of Pt-group/transition metal binary systems.

*Tensor representation.* We start from the CM [4, 7, 21], which represents a molecule  $\mathcal{M}$  as a symmetric atom-by-atom matrix  $\mathbf{M}_{i,j}$  with off-diagonal elements  $Z_i Z_j / d_{i,j}$ , where  $Z_i$  are nuclear charges and  $d_{i,j} = \|\mathbf{R}_i - \mathbf{R}_j\|$  is Euclidean distance between atoms  $i$  and  $j$ . To avoid dependence on atom order, which would violate (i),  $\mathbf{M}$  is sorted, causing discontinuities that violate (iii). Another shortcoming is the use of  $Z$ , which is not well suited for interpolation [22] as it overly decorrelates atoms from the same column of the periodic table.

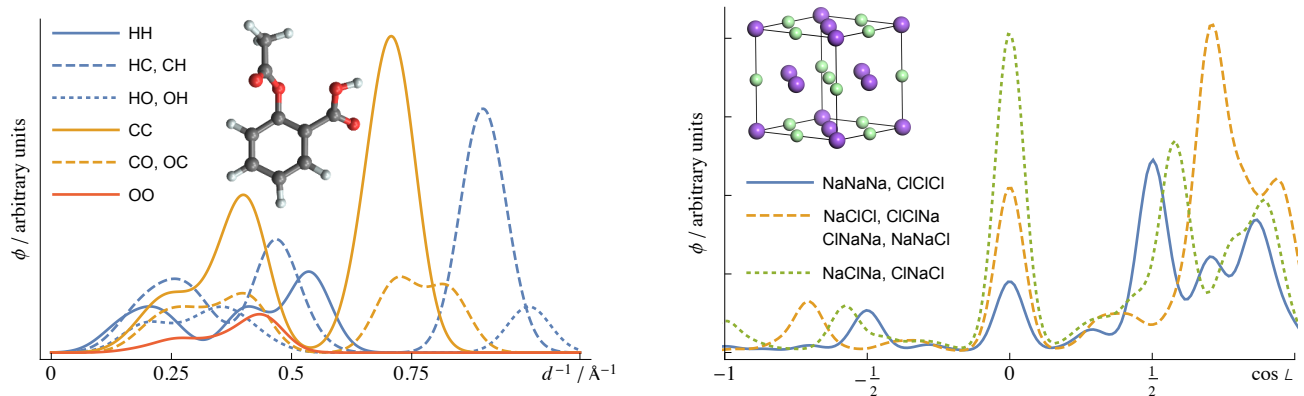


FIG. 1. Visualization of many-body tensor representation. Shown are distributions of inverse distances ( $k = 2$ , quadratic weighting) for aspirin ( $C_9O_4H_8$ , left), and, distributions of angles ( $k = 3$ , exponential weighting) for fcc salt (NaCl, right).

The related BoB [15] representation arranges the same terms differently. For each pair of elements, corresponding Coulomb terms are stored in sorted order, which can be viewed as an  $N_e \times N_e \times d$  tensor, or an  $N_e^2 \times d$  matrix by linearizing over element pairs, where  $N_e$  is number of chemical elements and  $d$  is sufficiently large. We retain stratification by elements, but avoid sorting by defining

$$f_{\text{BoB}}(x, z_1, z_2) = \sum_{i,j=1}^{N_a} \delta(x - d_{i,j}^{-1}) \delta(z_1, Z_i) \delta(z_2, Z_j), \quad (1)$$

a mixed continuous-discrete domain function encoding all (inverse) distances between pairs of elements. Here,  $N_a$  is number of atoms,  $\delta(\cdot)$  is Dirac’s delta, and  $\delta(\cdot, \cdot)$  is Kronecker’s delta. Arranging distances on a real-space axis removes the need for sorting.

For a smoother measure, we replace Dirac’s  $\delta$  with another probability distribution  $\mathcal{D}$ , “broadening” or “smearing” it [11, 23]. Adding a weighting function  $w_2$  and replacing the Kronecker  $\delta$  functions by an element correlation matrix  $C \in \mathbf{R}^{N_e \times N_e}$  yields

$$f_2(x, z_1, z_2) = \sum_{i,j=1}^{N_a} w_2(i, j) \mathcal{D}(x, g_2(i, j)) C_{z_1, Z_i} C_{z_2, Z_j} \quad (2)$$

of which (1) is a special case. In general,  $g_2$  describes a relation between atoms  $i$  and  $j$ ,  $\mathcal{D}$  broadens the result of  $g_2$  and places it on an axis, and  $w_2$  allows to weight down contributions, for example from far-away atoms. Here, we use the normal distribution  $\mathcal{D}(x, \mu) = (\sigma\sqrt{2\pi})^{-1} \exp(-(x - \mu)^2/2\sigma^2)$  throughout.  $f_2$  encodes two-body terms. Following recent work connecting ML with many-body expansions [17, 24], we generalize to

$$f_k(x, \mathbf{z}) = \sum_{\mathbf{i}=1}^{N_a} w_k(\mathbf{i}) \mathcal{D}(x, g_k(\mathbf{i})) \prod_{j=1}^k C_{z_j, Z_{i_j}}, \quad (3)$$

where  $\mathbf{z} \in \mathbf{N}^k$  are atomic numbers,  $\mathbf{i} = (i_1, \dots, i_k) \in \{1, \dots, N_a\}^k$  are index tuples, and  $w_k, g_k$  assign a scalar

to  $k$  atoms. [25] Canonical choices of  $g_k$  for  $k = 1, \dots, 4$  are atom counts, (inverse) distances, angles, and torsional angles. We measure similarity of two molecules as Euclidean distance between their representations,

$$d_k^2(\mathcal{M}, \mathcal{M}') = \sum_{\mathbf{z}} \int dx (f_k(x, \mathbf{z}) - f'_k(x, \mathbf{z}))^2. \quad (4)$$

In practice, we adjust Eq. 3 for symmetries. Discretizing the continuous axis yields a rank  $k + 1$  tensor of dimensions  $N_e \times \dots \times N_e \times N_x$ , where  $N_x = (x_{\max} - x_{\min})/\Delta x$ . Linearizing element ranks yields  $N_e^k \times N_x$  matrices, allowing efficient implementation via basic linear algebra subroutines [26, 27] as well as visualization (Fig. 1).

Periodic systems, used to model bulk crystals and surfaces, can be viewed as unit cells surrounded by infinitely many translated images of themselves. For such systems,  $N_a = \infty$  and the sum in (3) diverges. We prevent this by requiring an index of  $\mathbf{i}$  to be in the (same) primitive unit cell. [28] This accounts for translational symmetry and prevents double-counting. Use of weighting functions  $w_k$  such as exponentially decaying weights [29] then ensures convergence of the sum. Fig. 1 presents the resulting distribution of angles for fcc NaCl as an example. Note that the  $k$ -body terms  $g_k$  do not depend on choice of unit cell geometry (lattice vectors). This ensures unique representation of Bravais lattices where the choice of basis vectors is not unique, for example 2D hexagonal lattices where the angle between lattice vectors can be  $\frac{1}{3}\pi$  or  $\frac{2}{3}\pi$ .

*Results.* To validate the MBTR we demonstrate accurate predictions for properties of molecules and bulk crystals. Focusing on the representation, we employ plain kernel ridge regression ML models [5].

To demonstrate interpolation across *changes in chemistry of molecules* we employ a benchmark dataset [21] of 7k small organic molecules composed of up to seven C, N, O, S and Cl atoms, saturated with H. These molecules were relaxed to their ground state using the Perdew-Burke-Ernzerhof (PBE) [30, 31] approximation to Kohn-Sham density functional theory (DFT). Restriction to

TABLE I. *Prediction errors for small organic molecules.* Machine learning models of atomization energies  $E$  and isotropic polarizabilities  $\alpha$ , obtained at hybrid density functional level of theory, were trained on 5k molecules and evaluated on 2k others. RMSE=root mean square error, MAE=mean absolute error, CM=Coulomb matrix, BoB=bag of bonds, BAML=bonding angular machine learning, SOAP=smooth overlap of atomic positions, MBTR=many-body tensor representation. Best performance in bold face.

Repr.	Kernel	$E / \text{kcal mol}^{-1}$		$\alpha / \text{\AA}^3$	
		RMSE	MAE	RMSE	MAE
CM	Laplacian	5.48	3.54	0.18	0.13
BoB	Laplacian	3.32	1.95	0.13	0.09
BAML [17]	Laplacian	2.54	1.15	0.12	0.07
SOAP [35]	REMatch	1.61	0.92	0.07	0.05
MBTR	Linear	1.81	0.82	0.10	0.06
MBTR	Gaussian	<b>0.94</b>	<b>0.60</b>	<b>0.06</b>	<b>0.04</b>

relaxed structures projects out spatial variability and allows focusing on changes in chemistry alone. Table I presents prediction errors for atomization energies and isotropic polarizabilities obtained from single point calculations with the hybrid PBE0 [32–34] functional. For 5k training samples, prediction errors are below 1 kcal/mol (“chemical accuracy”), with the MBTR model’s mean absolute error of 0.6 kcal/mol corresponding to thermal fluctuations at room temperature. Note that MBTR achieves state-of-the-art performance already with a linear regression model, allowing constant-time predictions.

Interpolation across *changes in chemistry of crystalline materials* is demonstrated for a dataset of 11k elpasolite structures ( $ABC_2D_6$ ,  $AlNaK_2F_6$  prototype) [36][37] composed of 12 different elements, with geometries and energies computed at DFT/PBE level of theory. Predicting total energies with MBTR yields an RMSE of 7.3 meV/atom and MAE of 2.7 meV/atom (Fig. 2) for a training set size of 9k crystals. Adding elements and crystal structures should increase the intrinsic dimensionality of the learning problem, and thus prediction errors. To verify this, we created a dataset of 4616  $ABC_2$  ternary alloys containing the 26 non-radioactive elements of groups 1, 2, 13–15, spanning 6 rows and 5 columns of the periodic table. Structures were taken from the Open Quantum Materials Database (OQMD) [38, 39], with geometries and properties computed at the DFT/PBE level of theory as well. As expected, energy predictions exhibit larger errors (RMSE 34 meV/atom, MAE 24 meV/atom) compared to an elpasolite model with same training set size (RMSE 18 meV/atom, MAE 11 meV/atom).

For interpolation of *changes in geometry*, we employ a benchmark dataset [40, 41] of ab initio molecular dynamics trajectories of eight organic molecules. Each molecule was simulated at a temperature of 500 K for 150k to 1M time steps of 0.5 fs, with energies and forces computed at the DFT/PBE level of theory and the Tkatchenko–

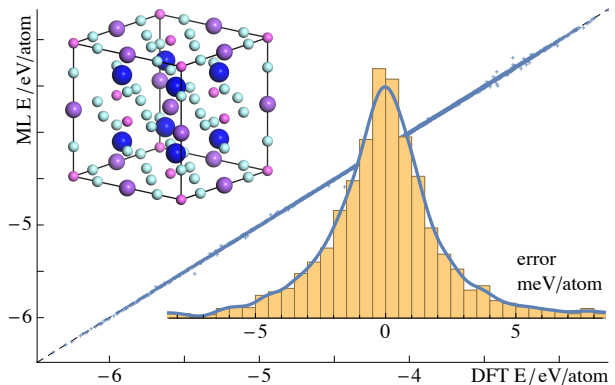


FIG. 2. *Total energy predictions for  $ABC_2D_6$  elpasolite structures* containing 12 different elements. Shown are reference energies (DFT  $E$ ) and predicted energies (ML  $E$ ), as well as distribution of errors (inset) for 2272 crystals, from a ML model trained on 9086 other ones.

TABLE II. *Prediction errors for changes in geometry of organic molecules.* MBTR models were trained on 10k random configurations from ab initio molecular dynamics simulations and evaluated on 2k other ones. Shown are prediction errors of total energies in kcal/mol. MAE=mean absolute error, RMSE=root mean squared error, DTNN=deep tensor neural network [40] trained on 50k configurations, GDML=gradient domain machine learning [41] trained on kernel matrices of size 27k–63k,  $CM^{md}$ =Coulomb matrix variant, MBTR=many-body tensor representation. Best MAE of last three representations in bold face.

Kernel	DTNN	GDML	$CM^{md}$		MBTR		MBTR	
	—	Matérn	Gaussian		linear		Gaussian	
Molecule	MAE	MAE	RMSE	MAE	RMSE	MAE	RMSE	MAE
benzene	0.04	0.07	0.10	0.07	0.08	<b>0.05</b>	0.08	0.06
uracil	—	0.11	0.33	0.23	0.54	0.29	0.62	<b>0.18</b>
naphthalene	—	0.12	0.51	0.39	0.50	<b>0.34</b>	0.50	0.38
aspirin	—	0.27	2.03	1.46	1.38	1.07	1.09	<b>0.80</b>
salicylic acid	0.50	0.12	0.71	0.53	0.65	0.47	0.53	<b>0.39</b>
malonaldehyde	0.19	0.16	0.61	0.45	0.79	0.58	0.51	<b>0.36</b>
ethanol	—	0.15	0.42	0.30	0.57	0.41	0.29	<b>0.20</b>
toluene	0.18	0.12	0.51	<b>0.38</b>	0.67	0.45	0.55	0.41

Scheffler model [42] for van der Waals interactions. Table II presents prediction errors for MBTR compared to deep tensor neural networks [40] and gradient domain ML [41]. MBTR models were trained on 10k configurations and validated on 2k other ones. The neural network was trained on a substantially larger set of 50k configurations. The gradient domain ML model employs a modified version  $CM^{md}$  of the CM, the Matérn kernel, and the gradient of the energy (forces) for training. The latter leads to kernel matrices of sizes between 27k and 63k. The  $CM^{md}$  column shows performance using our simple models and 10k training configurations. MBTR enables competitive predictions with sub-kcal/mol accuracy; again, performance of the linear model is close to the non-linear one.

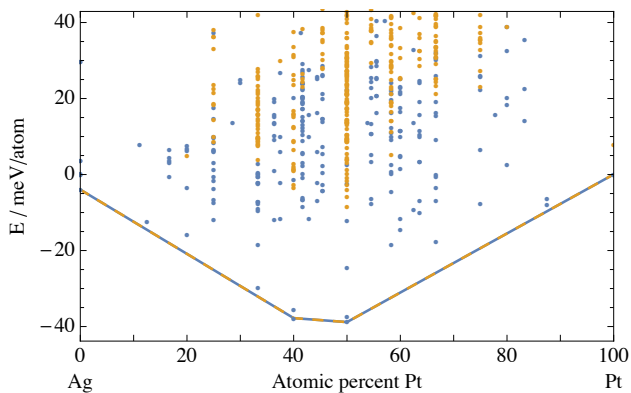


FIG. 3. *Applicability to phase diagrams of Pt-group/transition metal binary alloys.* Shown are convex hulls for  $\text{Ag}_x\text{Pt}_{1-x}$  based on all DFT calculations (blue dashed) and from active ML as a filter (orange dashed). The active learning model requested 266 DFT calculations (blue dots), saving 422 (61%) other ones (orange dots) and correctly identifying the convex hull. Note how low-energy structures are suggested for DFT, whereas high-energy ones are predicted.

We demonstrate *applicability* by using MBTR to identify stable and meta-stable states of Pt-group/transition metal binary alloys, relevant for industrial applications. For this, we employ a dataset [43] of 153 such alloys computed at DFT/PBE level of theory. The task is to identify the lowest-energy compositions forming the convex hull in a phase diagram. We treat alloys separately, a challenging scenario due to small training sets. Because of the resulting larger errors, directly using predicted energies leads to wrong convex hulls. However, using the ML model as a filter to exclude high-energy structures saves up to a third of all calculations. Adding a simple active learning [44] scheme allows saving half of all calculations while still identifying the correct convex hull. Fig. 3 presents results for AgPt. The active learning model requested 266 DFT calculations and predicted 422 (61%) other alloys, with a MAE of 33 meV/atom. The trade-off between number of saved calculations and probability of failing to identify the correct convex hull can be explicitly controlled.

*Discussion.* For CM and BoB, the Laplacian kernel performs better than the Gaussian kernel. [15, 45] It has been hypothesized [46] that this is due to the Laplacian kernels better ability to deal with the discontinuities of these representations. In agreement with this, we observe that for the continuous MBTR, the Gaussian kernel consistently performs better than the Laplacian kernel (supplement).

We use MBTR to represent whole molecules and crystals. With increasing size, and thus degrees of freedom, this approach is likely to degrade, and models exploiting locality via prediction of additive atomic energy contributions become appealing. [3, 47] These require representing local chemical environments [11], which MBTR should accommodate with appropriate modifications.

A limitation of the simple ML models used here is that they were trained only on energies. For technical reasons [48][49], differentiating such models can lead to errors in predicted forces. However, including reference forces, often provided by electronic structure calculations at no additional cost, into training [3, 41, 50] can reduce the number of reference calculations by an order of magnitude. [41] Training with forces would enable relaxation of structures, allowing to go from proof-of-principle presented here to applications such as virtual screening or crystal structure prediction.

We note in passing that problems in training of the ML models, such as outliers, could often be traced back to problems in the underlying reference calculations, such as unconverged fast Fourier transform grids or use of different settings (violating the assumption that a single function is being fitted), a phenomenon observed by others before. [51] This suggests that automated identification of errors in big datasets of electronic structure calculations via parametrization of ML models might be a general efficient approach for validation of such datasets. We rationalize this hypothesis by the fact that ML models identify regularity (correlations) in data, and faulty calculations deviating in some way from correct ones.

*Outlook.* The MBTR is a general numerical description of atomistic systems for rapid and accurate interpolation of quantum-mechanical calculations via ML, based on distributions of  $k$ -atom terms stratified by elements. Despite, or because of, this simple principle it is connected to many other representations, including Coulomb matrix [4], bag of bonds [15], histograms of distances, angles and dihedral angles [52], partial radial distribution functions [18], and moment tensor potentials [53], as well as to approaches like cluster expansion [54].

Advances in electronic structure codes and increasing availability of large-scale computing resources have led to big collections of ab initio calculations, such as the Materials Project [55], AFLOWlib [56], Open Quantum Materials Database [38, 39], and the Novel Materials Discovery Laboratory [57]. Enabled by efficient and effective representations like MBTR, models combining quantum mechanics with machine learning (QM/ML) for accurate interpolation could be key to exploration and exploitation in such “big data” settings.

MR and HH thank Matthias Scheffler for helpful discussions and support. MR thanks the Institute for Pure and Applied Mathematics (IPAM) for hospitality and support, participants of its program on Understanding Many-Particle Systems with Machine Learning for feedback, and Albert Bartók-Pártay, Gábor Csányi, Alexander Shapeev, Alexandre Tkatchenko and Alessandro de Vita for extended discussions. MR acknowledges funding from EU Horizon 2020 program grant 676580, The Novel Materials Discovery (NOMAD) Laboratory, a European Center of Excellence.

- 
- \* matthias.rupp@fhi-berlin.mpg.de; www.mrupp.info
- [1] M. I. Jordan and T. M. Mitchell, *Science* **349**, 255 (2015).
  - [2] R. Ramakrishnan, P. O. Dral, M. Rupp, and O. A. von Lilienfeld, *J. Chem. Theor. Comput.* **11**, 2087 (2015).
  - [3] A. P. Bartók, M. C. Payne, R. Kondor, and G. Csányi, *Phys. Rev. Lett.* **104**, 136403 (2010).
  - [4] M. Rupp, A. Tkatchenko, K.-R. Müller, and O. A. von Lilienfeld, *Phys. Rev. Lett.* **108**, 058301 (2012).
  - [5] M. Rupp, *Int. J. Quant. Chem.* **115**, 1058 (2015).
  - [6] R. Ramakrishnan, P. O. Dral, M. Rupp, and O. A. von Lilienfeld, *Sci. Data* **1**, 140022 (2014).
  - [7] M. Rupp, R. Ramakrishnan, and O. A. von Lilienfeld, *J. Phys. Chem. Lett.* **6**, 3309 (2015).
  - [8] A. P. Bartók, M. J. Gillan, F. R. Manby, and G. Csányi, *Phys. Rev. B* **88**, 054104 (2013).
  - [9] B. Schölkopf and A. Smola, *Learning with Kernels* (MIT Press, Cambridge, 2002).
  - [10] Kernel methods use a positive definite function (kernel) to implicitly define the Hilbert space. We focus on explicit numerical representations as input for vector kernels.
  - [11] A. P. Bartók, R. Kondor, and G. Csányi, *Phys. Rev. B* **87**, 184115 (2013).
  - [12] O. A. von Lilienfeld, R. Ramakrishnan, M. Rupp, and A. Knoll, *Int. J. Quant. Chem.* **115**, 1084 (2015).
  - [13] J. E. Moussa, *Phys. Rev. Lett.* **109**, 059801 (2012).
  - [14] C. R. Collins, G. J. Gordon, O. A. von Lilienfeld, and D. J. Yaron, arXiv, 1701.06649 (2017).
  - [15] K. Hansen, F. Biegler, R. Ramakrishnan, W. Pronobis, O. A. von Lilienfeld, K.-R. Müller, and A. Tkatchenko, *J. Phys. Chem. Lett.* **6**, 2326 (2015).
  - [16] J. Behler, *J. Chem. Phys.* **134**, 074106 (2011).
  - [17] B. Huang and O. A. von Lilienfeld, *J. Chem. Phys.* **145**, 161102 (2016).
  - [18] K. T. Schütt, H. Glawe, F. Brockherde, A. Sanna, K.-R. Müller, and E. K. Gross, *Phys. Rev. B* **89**, 205118 (2014).
  - [19] Z. Li, J. R. Kermode, and A. D. Vita, *Phys. Rev. Lett.* **114**, 096405 (2015).
  - [20] R. Todeschini and V. Consonni, *Handbook of Molecular Descriptors*, 2nd ed. (Wiley, Weinheim, Germany, 2009).
  - [21] G. Montavon, M. Rupp, V. Gobre, A. Vazquez-Mayagoitia, K. Hansen, A. Tkatchenko, K.-R. Müller, and O. A. von Lilienfeld, *New J. Phys.* **15**, 095003 (2013).
  - [22] L. M. Ghiringhelli, J. Vybiral, S. V. Levchenko, C. Draxl, and M. Scheffler, *Phys. Rev. Lett.* **114**, 105503 (2015).
  - [23] E. D. Cubuk, S. S. Schoenholz, J. M. Rieser, B. D. Malone, J. Rottler, D. J. Durian, E. Kaxiras, and A. J. Liu, *Phys. Rev. Lett.* **114**, 108001 (2015).
  - [24] K. Yao, J. E. Herr, and J. Parkhill, *J. Chem. Phys.* **146**, 014106 (2017).
  - [25] We use scalar geometry functions  $g_k$  for convenience; assigning vectors would simply increase the rank of the tensor. The product structure  $w_k(i)\mathcal{D}(x, g_k(i))$  allows efficient implementation as  $\mathcal{D}$  does not depend on  $\mathcal{M}$ .
  - [26] C. L. Lawson, R. J. Hanson, D. R. Kincaid, and F. T. Krogh, *ACM Trans. Math. Software* **5**, 308 (1979).
  - [27] L. S. Blackford, J. Demmel, J. Dongarra, I. Duff, S. Hammarling, G. Henry, M. Heroux, L. Kaufman, A. Lumsdaine, A. Petitet, R. Pozo, K. Remington, and R. C. Whaley, *ACM Trans. Math. Software* **28**, 135 (2002).
  - [28] Effectively representing one unit cell, including influence of surrounding cells on it, in accordance with computed properties being reported per cell.
  - [29] Exponential weighting was motivated by the exponential decay of screened Coulombic interactions in solids.
  - [30] J. P. Perdew, K. Burke, and M. Ernzerhof, *Phys. Rev. Lett.* **77**, 3865 (1996).
  - [31] J. P. Perdew, K. Burke, and M. Ernzerhof, *Phys. Rev. Lett.* **78**, 1396 (1997).
  - [32] J. P. Perdew, M. Ernzerhof, and K. Burke, *J. Chem. Phys.* **105**, 9982 (1996).
  - [33] M. Ernzerhof and G. E. Scuseria, *J. Chem. Phys.* **110**, 5029 (1999).
  - [34] C. Adamo and V. Barone, *J. Chem. Phys.* **110**, 6158 (1999).
  - [35] S. De, A. P. Bartók, G. Csányi, and M. Ceriotti, *Phys. Chem. Chem. Phys.* **18**, 13754 (2016).
  - [36] F. A. Faber, A. Lindmaa, O. A. von Lilienfeld, and R. Armiento, *Phys. Rev. Lett.* **117**, 135502 (2016).
  - [37] Dataset ABC2D6-16, available at <http://qmml.org>.
  - [38] J. E. Saal, S. Kirklin, M. Aykol, B. Meredig, and C. Wolverton, *J. Miner. Met. Mater. Soc.* **65**, 1501 (2013).
  - [39] S. Kirklin, J. E. Saal, B. Meredig, A. Thompson, J. W. Doak, M. Aykol, S. Rühl, and C. Wolverton, *Nat. Partn. J. Comput. Mater.* **1**, 15010 (2015).
  - [40] K. T. Schütt, F. Arbabzadah, S. Chmiela, K. R. Müller, and A. Tkatchenko, *Nat. Comm.* **8**, 13890 (2017).
  - [41] S. Chmiela, A. Tkatchenko, H. E. Sauceda, I. Poltavsky, K. Schütt, and K.-R. Müller, *Sci. Adv.* **3**, e1603015 (2017).
  - [42] A. Tkatchenko and M. Scheffler, *Phys. Rev. Lett.* **102**, 073005 (2009).
  - [43] G. L. Hart, S. Curtarolo, T. B. Massalski, and O. Levy, *Phys. Rev. X* **3**, 041035 (2013).
  - [44] B. Settles, *Active Learning*, Synthesis Lectures on Artificial Intelligence and Machine Learning, Vol. 18 (Morgan & Claypool, 2012).
  - [45] K. Hansen, G. Montavon, F. Biegler, S. Fazli, M. Rupp, M. Scheffler, O. A. von Lilienfeld, A. Tkatchenko, and K.-R. Müller, *J. Chem. Theor. Comput.* **9**, 3543 (2013).
  - [46] Gábor Csányi: Consequences of Discontinuities, CECAM/ $\Psi_k$  workshop “From Many-Body Hamiltonians to Machine Learning and Back”, Berlin, Germany, May 11–13, 2015.
  - [47] J. Behler, *Phys. Chem. Chem. Phys.* **13**, 17930 (2011).
  - [48] Differentiating an energy-based ML model can introduce noise due to small oscillations between training samples, whereas integrating a ML model of force removes noise.
  - [49] J. C. Snyder, M. Rupp, K. Hansen, K.-R. Müller, and K. Burke, *Phys. Rev. Lett.* **108**, 253002 (2012).
  - [50] A. Glielmo, P. Sollich, and A. D. Vita, arXiv, 1611.03877 (2016).
  - [51] Independent personal communications by Jörg Behler, Gábor Csányi, and Ekin Doğuş Çubuk.
  - [52] F. A. Faber, L. Hutchison, B. Huang, J. Gilmer, S. S. Schoenholz, G. E. Dahl, O. Vinyals, S. Kearnes, P. F. Riley, and O. A. von Lilienfeld, arXiv, 1702.05532 (2017).
  - [53] A. V. Shapeev, *Multiscale Model. Simul.* **14**, 1153 (2016).
  - [54] J. M. Sanchez, *Phys. Rev. B* **81**, 224202 (2010).
  - [55] A. Jain, S. P. Ong, G. Hautier, W. Chen, W. D. Richards, S. Dacek, S. Cholia, D. Gunter, D. Skinner, G. Ceder, and K. A. Persson, *APL Mater.* **1**, 011002 (2013).
  - [56] S. Curtarolo, W. Setyawan, G. L. W. Hart, M. Jahnatek, R. V. Chepulskii, R. H. Taylor, S. Wang, J. Xue, K. Yang, O. Levy, M. J. Mehl, H. T. Stokes, D. O. Demchenko, and D. Morgan, *Comput. Mater. Sci.* **58**, 218 (2012).
  - [57] NOvel MAterials Discovery (NOMAD) Laboratory, a European Center of Excellence; <https://nomad-coe.eu/>.

**Changes from v1:**

- Fig. 1a: Adjusted graph to directly reflect Eq. 3 for clarity by removing symmetry (double-counting) corrections.
- Fig. 1b: Changed x-axis units to  $\cos(\angle)$  used to generate the data and updated graph accordingly. Added cases ClNaNa and NaNaCl to legend.
- Added statement on symmetry corrections used in experiments after Eq. 4.
- Fig. 2: Changed “Formation energy” to “Total energy”, and corresponding changes in main text.
- Pg. 3: Removed half-sentence “substantially improving over the MAE of 100 meV/atom reported for a simpler representation” and associated footnote Ref. 38. This comparison was wrong as the quoted MAE referred to another set of elpasolites (I-VIII instead of III-VI used here).
- Added NOMAD funding to acknowledgments.
- Updated Ref. 24 (Yao et al), which appeared in J. Chem. Phys.
- Updated Ref. 42 (Chmiela et al), which appeared in Sci. Adv.